XVIII International Conference on Water Resources
CMWR 2010
J. Carrera (Ed)

PDF-APPROACH FOR MODELING DISSOLUTION-DRIVEN GRAVITY CURRENTS

Manav Tyagi* **and Patrick Jenny†**

*Institute of Fluid Dynamics, ETH Zurich
Sonneggstrasse 3, Zurich 8092, Switzerland,
e-mail: tyagi@ifd.mavt.ethz.ch, web page: http://www.ifd.mavt.ethz.ch

†Institute of Fluid Dynamics, ETH Zurich
Sonneggstrasse 3, Zurich 8092, Switzerland,
e-mail: jenny@ifd.mavt.ethz.ch, web page: http://www.ifd.mavt.ethz.ch

Key words: PDF-approach, porous media, dissolution, CO_2 storage

Summary. A probabilistic approach for modeling multi-phase flow with interfacial mass transfer is presented. With one- and two- dimensional simulations it is demonstrated that the PDF and Darcy modeling approaches give significantly different results. While the PDF-approach properly accounts for the long correlation length scales and the concentration variance in dissolution-driven gravity currents, this phenomenon cannot be captured accurately with a standard Darcy model.

1 INTRODUCTION

Carbon dioxide sequestration involves the capture and long term storage of CO_2 that would have been emitted into or remained in the atmosphere. Deep saline aquifers in the sedimentary basins are possible sites for long-term CO_2 storage [2, 1]. During the post-injection phase of CO_2 storage, due to the lower density of CO_2, the injected CO_2 plume migrates upwards and displaces the brine. During this upward motion of the CO_2 plume, several CO_2 trapping processes take place. In this paper, we focus on solubility trapping, which occurs due to slow dissolution of CO_2 into brine. Convective instability in the CO_2 rich brine leads to the formation of miscible fingers in the brine phase [3]. In order to upscale such scenarios from pore to Darcy scale, the size of REVs must be much larger than the finger size. However, if the finger size is of the order of Darcy scale, this poses a serious limitation on the validity of the Darcy-approach. Even if it is assumed that a well resolved Darcy based simulation provides a sufficiently accurate description of the large-scale flow, the presence of fingers puts a computational challenge for field scale simulations.

To model such unstable flow scenarios, we propose an alternative approach based on the evolution of a joint probability density function (PDF) of stochastic flow variables.

This PDF-approach requires Lagrangian evolutions for these stochastic variables. In a previous paper [4] we developed a stochastic particle method (SPM) for computing the evolution of joint-PDF of multi-phase flow in porous media. The particles in the SPM represent inifinitsimal fluid volumes with random flow variables as their properties and evolve such that their statistics represents the statistics of the physical fluid volumes.

2 STOCHASTIC MODEL

Here we develop the Lagrangian evolutions for the properties of stochastic particles based on the fine-scale physics of two-phase flow in porous media with interfacial mass transfer. Note that phase-1 (CO_2 phase) always remains in its pure state, but its only component (CO_2) dissolves into phase-2 (brine phase). Furthermore, it is assumed that the CO_2 density is constant and the density of brine weakly depends on the concentration of dissolved CO_2.

2.1 Position

A simple, yet quite general rule for the particle displacement in physical space is

$$d\boldsymbol{x}^* \;=\; \boldsymbol{u}^* dt \;+\; \sqrt{2\Gamma|\boldsymbol{u}^*|}d\boldsymbol{W}, \tag{1}$$

where $\boldsymbol{x}^*$ is the particle position, $\boldsymbol{u}^*$ the particle velocity, Γ a constant and $\boldsymbol{W}(t)$ a vector valued Wiener process. The first term on the right hand side accounts for the displacement due to the particle velocity and the second term models the pore scale dispersion with a dispersion coefficient proportional to the magnitude of the particle velocity.

2.2 Velocity

Dissolution leads to fine-scale variations of the brine density, i.e. the density ρ^* of the brine particles varies as a function of the local dissolved CO_2 concentration leading to buoyancy forces within the brine phase. A possible rule for the particle velocity is

$$\boldsymbol{u}^* \;=\; -\frac{k_{r_{a^*}} k}{S_{a^*}\phi\mu_{a^*}}(\boldsymbol{\nabla} p + \rho^* g \boldsymbol{e}_z) \tag{2}$$

where $k_{r_{a^*}}$, S_{a^*} and μ_{a^*} are the relative permeability, saturation and viscosity, respectively, of phase $a^* \in \{1, 2\}$. Further, ϕ is the porosity, p the average pressure, k the rock permeability and g the gravitational acceleration. Here the density ρ^* of the CO_2 particles is constant, i.e. $\rho^* = \rho_1$ and macroscopic capillary effects are ignored.

2.3 Interfacial mass transfer

We model dissolution by mass exchange between CO_2 and brine particles. For this purpose a concentration of CO_2 is defined as

$$c^* \;=\; \frac{m_c^*}{m^*}, \tag{3}$$

where m_c^* is the mass of CO_2 carried by the particle. Since the CO_2 phase remains in its pure state, $c^* = 1$ for all CO_2 particles.

2.3.1 Brine particles

The concentration of CO_2 in a brine particle can be altered either due to mass exchange with the CO_2 particles (dissolution) or due to mass exchange with other brine particles (molecular mixing). However, in the present paper the effect of molecular mixing of dissolved CO_2 in brine is ignored. It is assumed that the interfacial mass transfer is governed by the following first order rate law

$$\frac{dm^*}{dt} \;=\; -\frac{m^*}{\tau_d}(c^* - c^{eq}) \tag{4}$$

where τ_d is the dissolution time characterizing the time scale of dissolution process and c^{eq} is the equilibrium concentration of CO_2 in brine.

2.3.2 CO_2 particles

At any location and at any time the mass gained by the brine particles must be equal to the mass lost by the CO_2 particles. Here it is further assumed that at a given time all CO_2 particles of the same ensemble loose mass at a rate proportional to their own. This leads to the evolution

$$\frac{dm^*}{dt} \;=\; m^* \frac{\rho_2 S_2}{\rho_1 S_1} \frac{(\overline{c^*|a^*=2} - c^{eq})}{\tau_d}, \tag{5}$$

for the CO_2 particle. Note that $\overline{\cdot|a^*=1}$ and $\overline{\cdot|a^*=2}$ denote phase conditional Favre means.

2.4 Particle densities

For brine phase it is assumed that the particle density is a linear function of the dissolved CO_2 concentration. Thus, the density of a particle can be expressed as

$$\rho^* \;=\; \rho^0_{a^*} \;+\; \delta_{a^*2} \frac{\rho_2^{eq} - \rho_2^0}{c^{eq}} c^*, \tag{6}$$

where ρ_1^0 and ρ_2^0 are the phase densities in their pure states and ρ_2^{eq} is the equilibrium density.

2.5 Saturation and mean density

If a particle has mass m^* and volume v^* (such that $\rho^* = m^*/v^*$), the saturation S_α and the mean density ρ_α of phase α are defined as

$$S_\alpha \;=\; \frac{\langle v^* \delta_{a^*\alpha} \rangle}{\langle v^* \rangle} \quad \text{and} \quad \rho_\alpha \;=\; \frac{\langle m^* \delta_{a^*\alpha} \rangle}{\langle v^* \delta_{a^*\alpha} \rangle}, \tag{7}$$

where $\alpha \in \{1, 2\}$.

3 BOUSSINESQ APPROXIMATION

In many cases the flow model can greatly be simplified by a Boussinesq approximation, which implies that density variations are solely due to concentration variations in the brine (see Eq. (6)) and only needed to be considered in the gravity term. Otherwise, constants $\rho_1 = \rho_1^0$ and $\rho_1 = \rho_1^0$ are used. Here in particular, for further simplification, $\rho_1^0 = \rho_2^0 =$ constant is assumed.

3.1 Pressure equation and fractional flow

The Boussinesq approximation leads to the continuity equation $\boldsymbol{\nabla} \cdot \boldsymbol{F} = 0$, where the total volumetric flux $\boldsymbol{F} = \phi S_1 \overline{\boldsymbol{u}^* | a^* = 1} + \phi S_2 \overline{\boldsymbol{u}^* | a^* = 2}$ (for $\Gamma = 0$). Substituting for $\boldsymbol{F}$ using Eq. (2) leads to the elliptic equation (for $\Gamma = 0$)

$$-\boldsymbol{\nabla} \cdot \{\Lambda \boldsymbol{\nabla} p\} \quad = \quad g \boldsymbol{e}_z \cdot \boldsymbol{\nabla} \left\{ \frac{k k_{r_1}}{\mu_1} \rho_1 + \frac{k k_{r_2}}{\mu_2} \overline{\rho^* | a^* = 2} \right\} \tag{8}$$

for pressure, where $\Lambda = k k_{r_1}/\mu_1 + k k_{r_2}/\mu_2$ is the total flow mobility.

To solve transport problems, in particular if this is done with particle tracking, it is important to have a conservative scheme. To achieve this, we employ a fractional flow formulation for the particle velocities, i.e.

$$\boldsymbol{u}^* \;=\; \begin{cases} \frac{k_{r_1} k}{S_1 \mu_1 \phi \Lambda} \boldsymbol{F} \;+\; \frac{k^2 k_{r_1} k_{r_2} (\overline{\rho^* | a^* = 2} - \rho_1) g}{S_1 \mu_1 \mu_2 \phi \Lambda} \boldsymbol{e}_z & \text{if } \; a^* = 1 \\ \\ \frac{k_{r_2} k}{S_2 \mu_2 \phi \Lambda} \boldsymbol{F} \;+\; \frac{k^2 k_{r_1} k_{r_2} (\rho_1 - \rho^*) g}{S_2 \mu_1 \mu_2 \phi \Lambda} \boldsymbol{e}_z \;-\; \frac{k^2 k_{r_2}^2 (\rho^* - \overline{\rho^* | a^* = 2}) g}{S_2 \mu_2^2 \phi \Lambda} \boldsymbol{e}_z & \text{if } \; a^* = 2. \end{cases} \tag{9}$$

3.2 Multi-phase flow parameters and time scales

For the numerical simulations in this paper, we chose quadratic relative permeabilities, i.e. $k_{r_1} = S_1^2$ and $k_{r_2} = S_2^2$. Since the mass transfer rate due to dissolution depends on the saturation, it is assumed that τ_d is a function of CO_2 saturation and the relationship

$$\tau_d \;= \frac{\tau_0}{S_1} \tag{10}$$

is used. Note that there exist two kinds of buoyant forces in the present case: one due to the phase density difference, $\rho_2^0 - \rho_1^0$ and another due to density fluctuations within the brine. Estimates of the associated time scales are

$$\tau_g \;=\; \frac{\mu_2 \phi H}{k g (\rho_2^0 - \rho_1^0)} \quad \text{and} \quad \tau_\rho \;=\; \frac{\mu_2 \phi H}{k g (\rho_2^{eq} - \rho_2^0)}. \tag{11}$$

4 SIMULATION RESULTS

Next we present some one- and two- dimensional numerical results to demonstrate the difference between the PDF and the Darcy based modeling approaches. In the PDF-approach the SPM is employed, where a large number of computational particles are evolved via the Lagrangian equations presented in § 2. The total volume flux is the solution of Eq. (8), which is solved with a finite volume method. Note that the Darcy solution corresponds to having decorrelated particle properties in the SPM, i.e. ρ^* in Eq. (9) is replaced by $\overline{\rho^*|a^*=2}$. For the test cases, the post-injection phase of CO_2 storage is considered, i.e. a plume of lighter CO_2 migrates upwards in a confined aquifer filled with heavier brine. During the rise of the CO_2 plume some CO_2 dissolves into the surrounding phase, which results in a local increase of the brine density, thus leading to additional gravity currents within the brine phase. In all simulations the parameter τ_g/τ_ρ and the viscosity ratio μ_2/μ_1 are set equal to one. For the dissolution model we chose $c^{eq} = 0.1$ and $\tau_0 = 0.1\tau_g$.

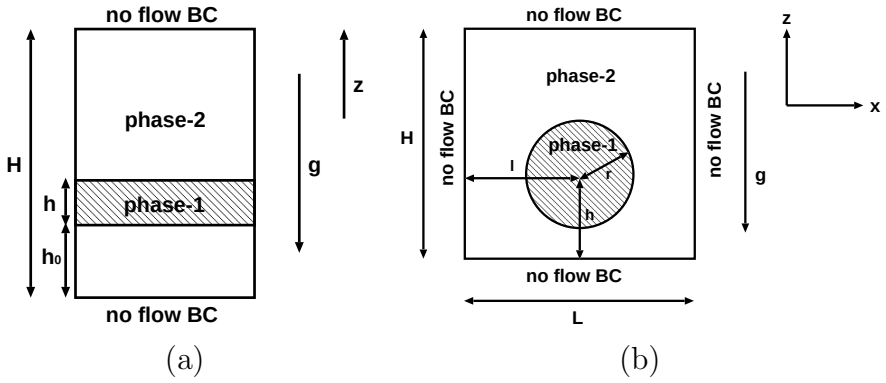

Figure 1: Geometry and initial distribution of the phases in (a) 1D test case and (b) 2D test case.

4.1 1D results

Here, a one-dimensional (1D) test case is considered, which represents a simplification of the rising CO_2 plume in a brine aquifer. The geometrical details and initial distribution of the phases are shown in figure 1a, where $h_0 = 0.1H$ and $h = 0.2H$. At $t = 0$, particles of equal mass and volume are uniformly distributed in the domain with $c^* = 1$ and $a^* = 1$ if $0.1H \leq z^* \leq 0.3H$ and $c^* = 0$ and $a^* = 2$, else. A grid with 100 equally spaced finite volumes ($\Delta z = 0.01H$) is employed to discretize the domain and a time step size of $\Delta t = 5 \times 10^{-3}\tau_g$ is used (the maximum CFL number in the domain is less than 0.5). In order to obtain smooth stochastic moments, $50,000$ particles per cell are employed in average.

Figure 2a depicts the spatial profiles of the conditional Favre mean concentration $\overline{c}$ =

$\overline{c^*|a^*=2}$ at $t=\tau_g$ obtained with the PDF and Darcy approaches. In the trailing region of the plume there is a significant difference between the average concentrations from the two approaches. The difference is essentially due to the stochastic formulation of phase-2 particle velocities (see Eq. (9)), i.e. the third term consisting of $\rho^* - \overline{\rho^*|a^*=2}$, which is absent in the Darcy model. The influence of this term can be quantified by the variance of concentration, i.e. $\sigma^2 = \overline{c^{*2}|a^*=2} - \overline{c^*|a^*=2}^2$. This is shown in figure 2b, where the time evolution of σ is plotted.

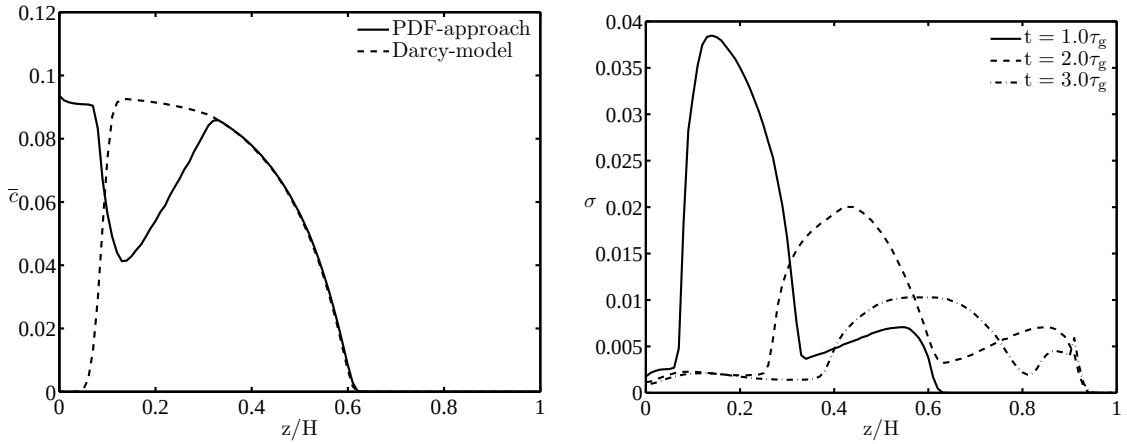

Figure 2: Comparison of the simulation results obtained with the PDF-approach and the Darcy-model: (a) Favre mean of the dissolved CO_2 concentration at $t=\tau_g$; (b) Favre standard deviation (σ) of the dissolved CO_2 concentration.

4.2 2D results

Next, we consider a two dimensional (2D) simulation test case, in which an initially circular plume of the lighter CO_2 phase rises upwards surrounded by the heavier brine. The geometrical details and initial configuration of the phases are shown in figure 1b, where $l=0.5L$, $h=0.25H$ and $r=0.2L$. At $t=0$, particles of equal mass and volume are uniformly distributed in the domain with $c^*=1$ and $a^*=1$ if $(x^*-l)^2+(z^*-h)^2 \leq r^2$ and $c^*=0$ and $a^*=2$ else. The domain is a square ($H/L=1$) filled with a homogeneous porous medium. A uniform orthogonal finite volume grid with 100×100 cells is employed to discretize the computational domain. The time step is chosen such that the CFL condition is satisfied everywhere. In order to obtain smooth stochastic moments, $4,000$ particles per cell are employed in average.

Similar to the 1D test case, a comparison between the results obtained with the two modeling approaches is presented. Figures 3a and 3b depict the total volume flux vectors at $t=2\tau_g$, where a clear difference can be seen between the dissolution-driven recirculation

zones. The PDF-approach predicts more lateral convection in the trailing region. A more significant difference can be observed between the concentration fields as shown in figures 4a and 4b, where the isolines of the Favre mean dissolved CO_2 concentration are plotted at the same time. The difference is mainly due to the stronger lateral convection in the trailing region with the PDF-approach.

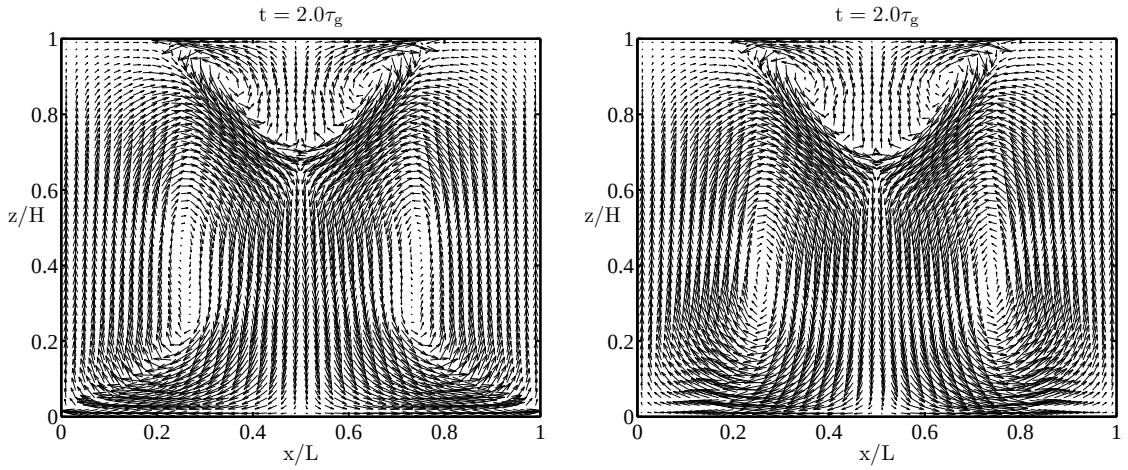

Figure 3: Total volume flux vectors at $t = 2\tau_g$ obtained with: (a) the PDF-approach; (b) the Darcy-model.

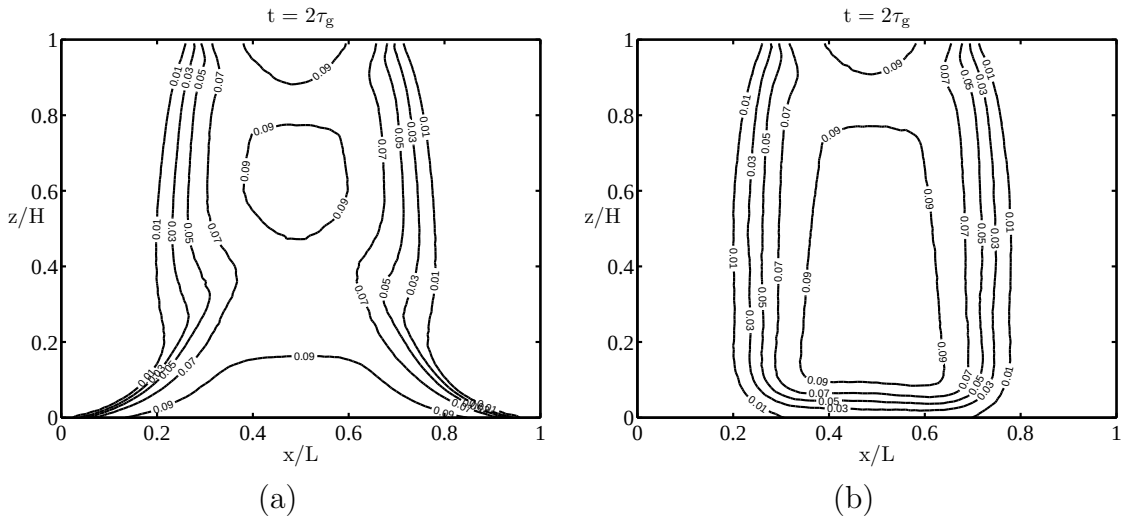

Figure 4: Favre mean concentration of dissolved CO_2 obtained with: (a) the PDF-approach; (b) the Darcy-model.

5 CONCLUSIONS

The potential of PDF-modeling approach to deal with non-equilibrium phenomena due to dissolution-driven gravity currents was demonstrated. It was shown that the results obtained with the PDF-approach significantly differ from those obtained with the Darcy-approach. The reason for this difference is the lack of information about the small scale dissolution-driven dynamics in the Darcy-model, which is very naturally captured in the PDF-approach. If the variance of CO_2 concentration in the brine phase is ignored, the PDF and Darcy simulations lead to the same results (except for the numerical inaccuracies).

REFERENCES

[1] S. Bachu. Sequestration of co2 in geological media in response to climate change: Capicity of deep saline aquifers to sequester co2 in solution. *Energy Conversion and Management*, 44:3151–3175, 2003.

[2] K. Pruess and J. Garcia. Multiphase flow dynamics during co2 disposal into saline aqifers. *Environmental Geology*, 42:282–295, 2002.

[3] A. Riaz, M. Hesse, H. A. Tchelepi, and F. M. Orr. Onset of convection in a gravitationally unstable diffusive boundary layer in porous media. *Journal of Fluid Mechanics*, 548:87–111, 2006.

[4] M. Tyagi, P. Jenny, I. Lunati, and H. A. Tchelepi. A stochastic, lagrangian modeling framework for multi-phase flow in porous media. *Journal of Computational Physics*, 227:6696–6714, 2008.